arXiv:1309.0291v1 [cond-mat.mtrl-sci] 2 Sep 2013

High-Symmetry Polarization Domains in Low-Symmetry Ferroelectrics

I. Lukyanchuk,[1] P. Sharma,[2] T. Nakajima,[3] S. Okamura,[4] J. F. Scott,[5] and A. Gruverman[2]
[1]*LPMC, University of Picardie Amiens, France and Landau Institute for Theoretical Physics, Russia*
[2]*Department of Physics and Astronomy, Nebraska Center for Materials and Nanoscience,*
University of Nebraska, Lincoln, NE 68588, USA
[3]*Institute of Materials Research, Tohoku University, Sendai, 980-8577 Japan*
[4]*Department of Applied Physics, Tokyo University of Science, Tokyo, 162-8601, Japan*
[5]*Cavendish Laboratory, 19 JJ Thomson Ave, Cambridge, UK*
(Dated: July 4, 2017)

We present experimental evidence for hexagonal domain faceting in the ferroelectric polymer PVDF-TrFE films having the lower orthorhombic crystallographic symmetry. This effect can arise from purely electrostatic depolarizing forces. We show that in contrast to magnetic bubble shape domains where such type of deformation instability has a predominantly elliptical character, the emergence of more symmetrical circular harmonics is favored in ferroelectrics with high dielectric constant.

PACS numbers: 77.80.Dj, 77.55.fp, 68.37.Ps

In nature, low-symmetry molecules often self-assemble to produce high-symmetry mesoscopic arrays or bundles of colloids, nanoparticles, proteins, and viruses [1]. Similar kind of mesoscopic self-assembly occurs for domain pattern formation in ferroelectric crystals. However, in most cases the symmetry of such domains is either the same or lower than the crystal symmetry and is fixed in space by the crystallographic axes.

There are, however, very few reports where domain faceting has a greater symmetry than that of the lattice or even incompatible with it. Triangular and hexagonal domains have been observed in lead germanate $Pb_5Ge_3O_{11}$ [2] and lithium niobate $LiNbO_3$ [3] crystals with 3-fold polar axes. Relaxation of initially circular domains into pentagonal and hexagonal ones was also reported in [111]-oriented lead zirconate-titanate $Pb(Zr,Ti)O_3$ films [4]. In some cases these effects occur under external perturbation, such as laser or e-beam irradiation. A 6-fold pattern in laser-irradiated ferroelectric of $PbMg_{1/3}Nb_{2/3}O_3$, which has a purely cubic symmetry, was observed by Scott *et al.* [5, 6]. In earlier studies, Schwarz and Hora reported the 6-fold diffraction patterns appearing along a 2-fold axis in quartz irradiated simultaneously by e-beams and blue laser light [7, 8]. Brown and Hollingsworth reported domain structures in thiourea compounds with 12-fold symmetry in spite of the fact that the crystals had only 2-fold lattice symmetry [9]. A peculiar kind of hexagonal domain crystallization has been observed in sodium dodecyl sulfate surfactant [10], but there is only a rather general understanding of these phenomena.

In this work, we present new data on hexagonal domain formation in the ferroelectric co-polymer of poly(vinylidene fluoride-trifluoroethylene (PVDF-TrFE) that lacks any hexagonal lattice symmetry. We interpret our data in terms of the electrostatic depolarization instability-theory developed by Thiele [11] to depict the elliptical deformation of small circular domain patterns in ferromagnetic bubble-memory devices [12, 13]. However, unlike magnetic bubbles, ferroelectric PVDF-TrFE favors the hexagonal faceting instability.

PVDF-TrFE is the best known ferroelectric polymer widely used due to its relatively high polarization and piezoelectric parameters [14]. Discovery of ferroelectricity in ultrathin PVDF-TrFE films [15] and fabrication of highly ordered nanomesas arrays for non-volatile memories [16] draw additional attention due to possibility of integration of these materials into all-organic electronic systems. It remains a model material for investigation of the mechanism of polarization reversal in organic ferroelectrics.

The PVDF-TrFE (75/25) copolymer films have been

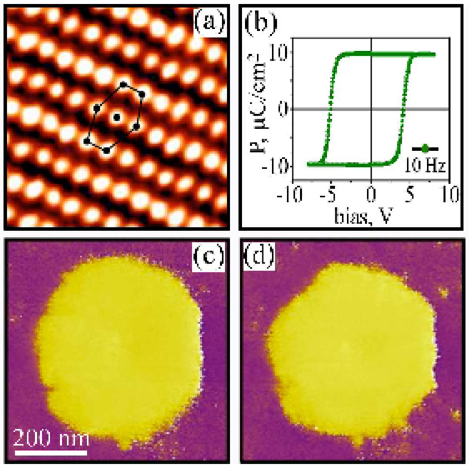

FIG. 1: (a) An atomically-resolved STM image of the surface of PVDF-TrFE film at room temperature (Reprinted with permission from [17]. (b) Polarization hysteresis loop of PVDF-TrFE film. (c) PFM image of the domain written by a -55 V, 1s pulse applied by a PFM tip. (d) PFM image of the same domain 15 minutes after pulse application.

fabricated by spin-coating the VDF/TrFE solution dissolved in diethyl carbonate (3 wt%) on the (111) Pt-sputtered (150 nm) on Ti(5 nm)/SiO$_2$(200 nm)/Si substrate followed by annealing at 120 °C. The thickness of the PVDF-TrFE film is 50 nm. X-ray θ-2θ scans showed a clear peak at 19.7°, which corresponded to (110) d-spacing of the all-trans ferroelectric β-phase [18]. The (110) peak pointed out to the highly textured PVDF-TrFE molecular chains lying parallel to the substrate.

A commercial atomic force microscope (Asylum MFP-3D) has been used to generate and visualize the domain structure in the piezoresponse force microscopy (PFM) mode. Domain visualization has been performed by applying 1.5 V modulating voltage in the $200 - 400$ kHz frequency range to the Pt-Ti-coated silicon cantilevers. We used a ferroelectric test system (Radiant system) to record the $P - E$ hysteresis loops from the Au top electrodes deposited by thermal evaporation.

Ferroelectric polarization in PVDF-TrFE arises from alignment of molecular dipoles formed by electropositive hydrogen and electronegative fluorine atoms. The all-trans (β-phase) molecular conformation results in the dipoles being oriented nearly perpendicular to the chain axis and polarization reversal is associated with rotation of these dipoles about the molecular chains. In the crystalline β-phase of highly textured PVDF-TrFE, molecules tend to pack parallel to each other forming a structure with the orthorhombic symmetry $Cm2m$ (C_{2v}^{14}) space group, with 2-fold polar axis nearly perpendicular to the film's plane. In Fig.1a, it can be seen that the molecular chains arranged themselves in parallel rows, forming a quasihexagonal close packing structure [17].

Preliminary PFM testing showed that the as-grown PVDF-TrFE films were uniformly polarized downward. Polarization loops were shifted horizontally toward the negative voltage (Fig.1b) suggesting a presence of an internal built-in electric field oriented toward the substrate. This field could be estimated from the polarization loop asymmetry as $E = (|V_c^+| - |V_c^-|)/\varepsilon h \simeq 10^5$ V/cm, where V_c^-, and V_c^+ are negative and positive coercive voltages, respectively, $h \simeq 50$ nm is film thickness and $\varepsilon \simeq 15$ is the dielectric permittivity [14]. Figures 1c,d illustrate the domain faceting effect observed in these films. A voltage pulse in the range from -15 V to -60 V applied to the PFM tip results in a single circular domain with radius r of about $50 - 250$ nm (Fig.1c) with polarization oriented against the imprint. After the field is off, the domain starts to slowly relax back acquiring a hexagonal shape during the process (Fig.1d).

We show that both the domain contraction and tendency to expand its perimeter via faceting instability are provided by the purely electrostatic force balance.

It is known that the depolarizing effect of surface charges due to discontinuity of polarization vector at the interface plays the critical role in the formation and dynamics of ferroelectric domains. However, the foreseeable periodic Landau-Kittel domain structure [19, 20] with expected half-period $d \simeq (h\xi_0)^{1/2} \simeq 10$ nm (where $\xi_0 \simeq 2$ nm is the coherence length) was not observed in these PVDF-TrFE films. Most probably, this is due to the fact that the depolarization field is initially screened by accumulation of the charged species at the top surface and by the charge carriers of the conductive electrode at the bottom of the film.

During application of the switching pulse by the PFM tip, the surface screening charges in the vicinity of the tip are dispersed, activating the depolarization forces in the area of the newly-generated domain. Subjected to electrostatic tension, which could also stem from the internal built-in field, this domain starts to relax until it is stabilized by the redistributed surface screening charges.

To account for the forces, acting on the generated domain just after its creation and to reveal the faceting instability, we, following [11], distinguish three contributions to the energy W_r of cylindrical domain:

$$W_r = W_{dw} + W_{PE} + W_d \tag{1}$$

(i) W_{dw} is the domain wall (DW) energy, which is provided by DW surface tension $\sigma_{dw} = \varepsilon^{-1}\left(4\pi P^2\right)\xi_0$:

$$W_{dw} \simeq \varepsilon^{-1}\left(4\pi P^2\right)\xi_0\left(2\pi r\right)h. \tag{2}$$

However, the W_{dw} is at least of $\xi_0/h \simeq 25$ times smaller than two other contributions (unlike in magnetic domains where $\xi_0 \sim 50nm$) and can be neglected in electrostatic calculations.

(ii) W_{PE} is the energy of polarization interaction with the electrical field E, which in our case of the relaxing domain is the internal built-in imprint field:

$$W_{PE} = 2\left(\pi r^2 h\right)PE. \tag{3}$$

This contribution is proportional to the domain volume $\pi r^2 h$ and factor 2 is introduced because of the domain re-polarization.

(iii) W_d is the depolarization energy, which is determined by the surface charge of density $\sigma = \pm P$ due to polarization termination at the film surface. To outline how this contribution drives the domain shape instability we note that W_d is nothing else, but the energy excess of the cylindrical capacitor with the plate charges $Q = \pm\left(2P\right)\pi r^2$ which is oppositely polarized with respect to the original ferroelectric slab. Capacitance of such finite-size capacitor with $\varepsilon = 1$ was first calculated by Kirchhoff in 1877 [21] in the limiting case of $r \gg h$ and two years later generalized by Lorentz [22] in terms of the elliptic function for arbitrary aspect ratio h/r. In late of 1960's, Thiele performed similar calculations for the energy of the cylindrical magnetic domain [11], but again with $\varepsilon = 1$ [23]. We summarize their results for the case of $r \gg h$ as:

$$W_{d1} \simeq -\left(2\pi r\right)h^2\left(2P\right)^2\ln\frac{8r}{e^{1/2}h}, \tag{4}$$

where $e \simeq 2.71$ and the index "one" means $\varepsilon = 1$ [23].

Expression (4) is similar to the well known energy of the edge fringing field of the finite-size capacitor [21, 22]. Importantly, the negative sign of W_{d1} is explained by the repulsion of the edge-forming dipoles. Caused by the long-range electrostatic forces, this term is not simply proportional to the DW surface, like but also contains the non-local logarithmic correction, dependent on the integral domain shape. Acting against W_{PE} which minimizes the domain volume, it determines the tendency of DW to increase its surface by either faceting or roughening deformations.

The size and shape of domain is, therefore, the result of a balance between contributions of different terms in Eq.(1). The comprehensive analysis of possible domain instabilities has been carried out by Thiele for ferromagnetic materials, which are characterized by the almost uniform permittivity [11]. To apply these results to ferroelectric films, one has to find out how Thiele's approach can be generalized for the case of the films with arbitrary dielectric constant $\varepsilon > 1$.

Let us consider two dipoles with charges $\pm q$, located across the slab of permittivity ε and thickness h and separated by a distance ρ. Their interaction energy can be calculated as [24]:

$$W_{d\varepsilon} = -\frac{4\varepsilon^2}{\varepsilon^2 - 1} \sum_{n=1}^{\infty} (-\beta)^n \, W_{1d}(nh), \quad \beta = \frac{\varepsilon - 1}{\varepsilon + 1}, \quad (5)$$

where $W_{d1}(h) = 2q^2 \left[r^{-1} - \left(h^2 + \rho^2 \right)^{-1/2} \right]$ is the energy of dipolar interaction in vacuum at $\varepsilon = 1$. Since each domain can be considered as an ensemble of interacting parallel dipoles, Eq.(5) can also be used to find the depolarization energy of such a domain $W_{d\varepsilon}$ for an arbitrary value of ε if its energy W_{d1} is known for $\varepsilon = 1$.

Using summations $\sum_{n=1}^{\infty} n^2 (-\beta)^n = -\frac{\varepsilon^2 - 1}{4\varepsilon^3}$ and $c_\varepsilon = \frac{4\varepsilon^2}{\varepsilon^2 - 1} \sum_{n=1}^{\infty} (-\beta)^n \, n^2 \ln n \overset{\varepsilon \gg 1}{\simeq} 0.84$, we transform Eq.(4) to:

$$W_{d\varepsilon} \simeq -\left(2\pi r\right) h^2 \left[\frac{1}{\varepsilon^2} \ln \frac{8r}{e^{1/2} h} + \frac{c_\varepsilon}{\varepsilon} \right] \left(2P\right)^2 . \quad (6)$$

Transformation (5) is valid for a single domain in a free-standing ferroelectric film. To account for the influence of conducting substrate, one should apply the mirror boundary condition, provided by one more transformation $W_d(h) \to \frac{1}{2} W_d(2h)$ that we shall use at the end.

The equilibrium domain radius is given by the minimum of the energy $W_{PE} + W_{d\varepsilon}$. A closer look at Eqs (3) and (6) reveals that this minimum lies well below the actual radius, at $r \ll h$ and is comparable to the Kittel domain width $d \simeq 10$ nm. This explains the tendency of the newly created domain to relax via viscous contraction.

To take into consideration the possibility of shape-breaking instability during relaxation process we parameterize the domain boundary in polar coordinates as $R = R(\theta)$ and, following [11], account its deviation from the cylinder with $R = r$ by emergence of circular harmonics:

$$R(\theta) = r + \sum_{k=2}^{\infty} \left(\Delta r_k\right) \cos k\theta, \quad (7)$$

with small amplitudes $|\Delta r_k| \ll r$.

To address the question of domain stability under perturbation (7) we, following [11], expand the variation of the energy as:

$$W = W_r + \frac{1}{2} \sum_{k=2}^{\infty} \left[W''_{PE} + W''_d(k) \right] \left(\Delta r_k\right)^2 , \quad (8)$$

where

$$W''_{PE} = \frac{1}{2} \frac{\partial^2 W_{PE}}{\partial r^2} = 2\pi h P E \quad (9)$$

is the harmonics interaction with imprint field and $W''_d(k)$ is the depolarization field contribution. For $\varepsilon = 1$ and in the limit $r \gg h$ this term was calculated in [11] as:

$$W''_{d1}(k) \simeq -\pi \left(2P\right)^2 \frac{h^2}{r} k^2 \ln \frac{8er}{kh}, \quad (10)$$

Here, we neglected the DW energy contribution as mentioned above.

A cylindrical domain is unstable with respect to axial symmetry-breaking modes if the corresponding coefficients in (8) are negative:

$$W''_{PE} + W''_d(k) < 0. \quad (11)$$

The instability comes from the negative logarithmic term in (10). However to explore the instability condition (11) we should generalize the expression (10) for arbitrary $\varepsilon > 1$ using the transformation (5). Summing the log-terms in lowest in h/r order we obtain:

$$W''_{d\varepsilon}(k) = -\frac{\pi h^2}{r} \left[\frac{1}{\varepsilon^2} \ln \frac{8er}{kh} + \frac{c_\varepsilon}{\varepsilon} \right] \left(2P\right)^2 k^2. \quad (12)$$

Now using the transformation: $W''_{d\varepsilon}(k, h) \to \frac{1}{2} W''_{d\varepsilon}(k, 2h)$ we include the effect of the bottom electrode and arrive at the instability condition:

$$\frac{\varepsilon E}{P} \frac{r}{(2h)} < 2k^2 \left[\frac{1}{\varepsilon} \ln \frac{8er}{k(2h)} + c_\varepsilon \right], \quad (13)$$

For $\varepsilon \gg 1$, we can neglect the log term and reduce condition (13) to the simpler form: $\frac{\varepsilon E}{P} \frac{r}{h} < 3.4k^2$.

Graphic analysis shown in Fig.2 reveals that the shape-breaking instability develops first for the high k-modes, which have a *higher* symmetry than the crystal background. Notably, for a domain with initial radius $r \simeq 4h \simeq 200\,\text{nm}$, the hexagonal faceting instability with

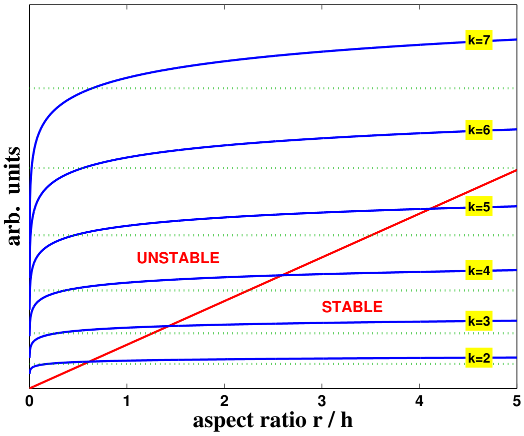

FIG. 2: Graphical solution of instability condition (13) for PVDF film with $\varepsilon \simeq 15$ [14], $\varepsilon E/P \simeq 1.6$ as function of the aspect ratio r/h. Dotted lines present the approximate solutions for high ε.

$k = 6$ can occur, whereas the modes with $k < 4$ and, in particularly, elliptic deformation with $k = 2$, compatible with two-fold symmetry of PVDF-TrFE are electrostatically protected. The situation is quite different from the magnetic case were the elliptical instability is the most favorable one [11, 12]. The reason is that, the domain formation in ferroelectrics is stabilized by the bulk field-interaction term (3) whereas the DW surface-tension term (2) appears to be more relevant in ferromagnets.

However, to know which of the electrostatically allowed symmetry-breaking modes is unstable during domain relaxation we should go beyond the linear-stability analysis, since several factors are coming into the play. For instance, the DW pinning in the atomic planes shown in Fig.1a can be critical for the mode selection. Minimization of the anisotropic pinning energy, know as Wulff construction [25], acting along with the high-k electrostatic instability, can favor selection of those surfaces that are most close to the perfect hexagonal faceting.

The dynamic buckling effects during domain contraction can also favor the particular (hexagonal) shape-breaking as was shown, for example, for the case of the relaxing drops in dipolar ferrofluids [26].

To conclude, we have discovered hexagonal faceting of domains in ferroelectric polymer PVDF-TrFE films, which have symmetry much lower than hexagonal. We interpret this effect in terms of the electrostatic depolarization instability originally used by Thiele for magnetic bubble domains. Unlike magnetic bubbles with the $k = 2$ elliptical instability, ferroelectrics favor the instability with higher-k modes. Our analysis raises questions about the origin of high-symmetry domain faceting in $Pb_5Ge_3O_{11}$ [2] and PZT [4] ferroelectrics. The described approach can be applied to a wider range of instabilities in quite unrelated materials, including 6-fold faceting in surfactants [10] and in thiourea inclusion compounds with $k = 12$ [9].

[1] S. C. Glotzer, Science **337**, 453 (2012)
[2] V. Ya. Shur, A. Gruverman, V. V. Letuchev *et al.*, Ferroelectrics, 98, **29** (1989)
[3] D. A. Scrymgeour, V. Gopalan, A. Itagi,*et al.*, Phys. Rev. B **71**, 184110 (2005)
[4] C. S. Ganpule, A. L. Roytburd, V. Nagarajan, *et al.*, Phys. Rev. **B 65**, 014101 (2002))
[5] J. F. Scott, R. A. O'Sullivan, Nature **382**, 305 (1996)
[6] J. F. Scott, R. A. O'Sullivan, and M. H. Reich, Physica **A 233**, 655 (1996)
[7] H. Schwarz and H. Hora, Appl. Phys. Lett. **15**, 349 (1969)
[8] H. Schwarz, Nature **225**, 1173 (1970)
[9] M. E. Brown and M. D. Hollingsworth, Nature **376**, 323 (1995)
[10] J.-M. Flesselles, M. O. Magnasco, and A. Libchaber, Phys. Rev. Lett. **67**, 2489 (1991
[11] A. A. Thiele, Bell System Techn. J. **48**, 3287 (1969) and ibid. **50**, 711 (1971)
[12] For review see: A. P. Malozemoff and J. C. Slonczewski, Magnetic domain walls in bubble materials, Academic Press, 1979
[13] A similar elliptic instability of polarization domains was observed also in lipid monolayers; See e.g.: D. J. Keller, J. P. Korb and H. M. McConnell, J. Phys. Chem. **91**, 6417 (1987)
[14] A. Lovinger, Science **220**, 1115 (1983)
[15] S. Ducharme, V. M. Fridkin, A. V. Bune *et al.*, Phys. Rev. Lett. **84**, 175 (2000)
[16] Z. Hu, M. Tian, B. Nysten and A. M. Jonas, Nature Mater. **8** 62 (2009)
[17] L. Cai, H. Qu, C. Lu, S. Ducharme, P. A. Dowben, and J. Zhang, Phys. Rev. B **70**, 155411 (2004)
[18] M. Bai and S. Ducharme, Appl. Phys. Lett. **85**, 3528 (2004)
[19] L. Landau and E. Lifshitz, Phys. Z. Sowjet. **8**, 153 (1935)
[20] C. Kittel, Phys. Rev. **70**, 965 (1946)
[21] G. Kirchhoff, Monatsb. Deutsch. Akad. Wiss. Berlin, pp. 144-162 (1877); see also L. D. Landau and E. M. Lifshitz, *Electrodynamics of Continuous Media* (Elsevier, New York,1985)
[22] L. Lorentz, Wied. Ann. **7**, 161 (1879)
[23] The edge-fringing energy for ferroelectric domain was calulated in A. M. Bratkovsky and A. P. Levanyuk, Phys. Rev. Lett. **85**, 4614 (2000) for particular, different from our case when ε inside and outside the film are comparable.
[24] See supplementary material for technical derivation of dipolar interaction energy (5).
[25] G. Wulff, Zeitschrift für Krystallographie und Mineralogie, **34**, 449 (1901)
[26] S. A. Langer, R. E. Goldstein, D. P. Jackson, Phys. Rev. B **46**, 4894 (1992)

SUPPLEMENTARY MATERIAL

Dipolar Interaction via Dielectric Slab

We calculate the interaction energy of two dipoles, located across the dielectric slab of thickness h and permittivity ε at distance ρ from each other, as shown in Fig. 3. The coordinate system (x, y, z) is placed in the center of the first dipole, axis $\mathbf{z}$ being directed downward, perpendicular to the slab and axis $\mathbf{x}$ being in the direction of the second dipole. The coordinates of the top charge $q_t^{(1)} = +q$ and of the bottom charge $q_b^{(1)} = -q$ of the first dipole are $\mathbf{R}_t^{(1)} = (0, 0, -h/2)$ and $\mathbf{R}_b^{(1)} = (0, 0, h/2)$ correspondingly. The corresponding coordinates of the top and bottom charges of the second dipole, $q_t^{(2)} = +q$ and $q_b^{(2)} = -q$, are $\mathbf{R}_t^{(2)} = (\rho, 0, -h/2)$ and $\mathbf{R}_b^{(2)} = (\rho, 0, h/2)$.

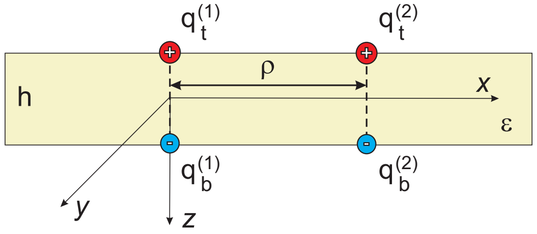

FIG. 3: Dipolar location geometry and coordinate system

Let us consider the field due to the upper positive charge of the first dipole $q_t^{(1)} = +q$. The distribution of the electrostatic potential inside the slab can be presented by the integral relation, involving the zero-order Bessel function $J_0(r_\perp)$ [1] :

$$\varphi_t^{(1)} = \int_0^\infty \left[B_1(k) e^{-k\left(z+\frac{h}{2}\right)} + B_2(k) e^{k\left(z+\frac{h}{2}\right)}\right] J_0(kr_\perp) dk, \tag{14}$$

with $r_\perp = (x^2 + y^2)^{1/2}$, $-\frac{h}{2} < z < \frac{h}{2}$,

$$B_1 = q\frac{(1-\beta)}{1-\beta^2 e^{-2kh}}, \quad B_2 = q\frac{\beta(1-\beta)e^{-2kh}}{1-\beta^2 e^{-2kh}} \tag{15}$$

and

$$\beta = \frac{\varepsilon - 1}{\varepsilon + 1}. \tag{16}$$

Substitution of B_1 and B_2 into (14) gives:

$$\varphi_t^{(1)} = q(1-\beta)\int_0^\infty \frac{e^{-k\left(z+\frac{h}{2}\right)} + \beta e^{k\left(z-\frac{3h}{2}\right)}}{1-\beta^2 e^{-2kh}} J_0(kr_\perp) dk. \tag{17}$$

Similarly, the distribution of potential of the bottom negative charge of the first dipole $q_b^{(1)} = -q$ can be written as $\varphi_b^{(1)}(r_\perp, z) = -\varphi_t^{(1)}(r_\perp, -z)$ and the resulting potential distribution of the first dipole $\varphi_d^{(1)} = \varphi_t^{(1)} + \varphi_b^{(1)}$ as:

$$\varphi_d^{(1)} = q(1-\beta)\int_0^\infty \frac{e^{-kz} - e^{kz}}{1+\beta e^{-kh}} e^{-kh/2} J_0(kr_\perp) dk. \tag{18}$$

The electrostatic energy of interaction between first and second dipole is calculated as:

$$\begin{aligned} W_{d\varepsilon} &= \varphi_d^{(1)}(\mathbf{R}_t^{(2)})\, q_t^{(2)} + \varphi_d^{(1)}(\mathbf{R}_b^{(2)})\, q_b^{(2)} \\ &= 2q^2(1-\beta)\int_0^\infty \frac{1-e^{-kh}}{1+\beta e^{-kh}} J_0(k\rho) dk. \end{aligned} \tag{19}$$

To simplify Eq.(19) we expand the denominator in series:

$$\frac{1}{1+\beta e^{-kh}} = \sum_{n=0}^\infty (-\beta)^n e^{-khn} \tag{20}$$

and integrate the resulting expression, using the formula:

$$\int_0^\infty e^{-k\lambda} J_0(k\eta) dk = \frac{1}{(\eta^2+\lambda^2)^{1/2}}, \quad \lambda > 0. \tag{21}$$

After some algebra, taking into account that $\sum_{n=1}^\infty (-\beta)^n = -\left(1+\beta^{-1}\right)^{-1}$, we obtain

$$\begin{aligned} W_{d\varepsilon}(h) &= 2q^2(1-\beta)\left[\frac{1}{r} + \sum_{n=1}^\infty \frac{\left(1+\beta^{-1}\right)(-\beta)^n}{(\rho^2+n^2h^2)^{1/2}}\right] \\ &= -\frac{4\varepsilon}{\varepsilon^2-1}\sum_{n=1}^\infty (-\beta)^n W_{d1}(nh), \end{aligned} \tag{22}$$

where

$$W_{d1}(h) = 2\left[\frac{q^2}{\rho} - \frac{q^2}{(\rho^2+h^2)^{1/2}}\right] \tag{23}$$

is the energy of dipolar interaction in vacuum at $\varepsilon = 1$.

---

[1] See the problem 3.81 in V. V. Batygin, I. N. Toptygin and D. ter Haar, *Problems in Electrodynamics*, Academic Press, 1978 (ISBN 0-12-082160-5) with $a = 0$, $c = h$ and with shift of the coordinate center to the middle of the plate, $z \to z + h/2$.